Supplementary Material (ESI) for PCCP

Supporting Information

On the origin of an unusual dependence of chemical reactivity of ferric (hydr)oxides on nanoparticle size

I.V. Chernyshova, S. Ponnurangam, and P. Somasundaran

NSF I/UCRC Center for Particulate & Surfactant Systems (CPaSS), Columbia University, New York, 10027 NY

Effect of NP size on sorption of Cu(II) and U(VI) by hematite NPs[1, 2]

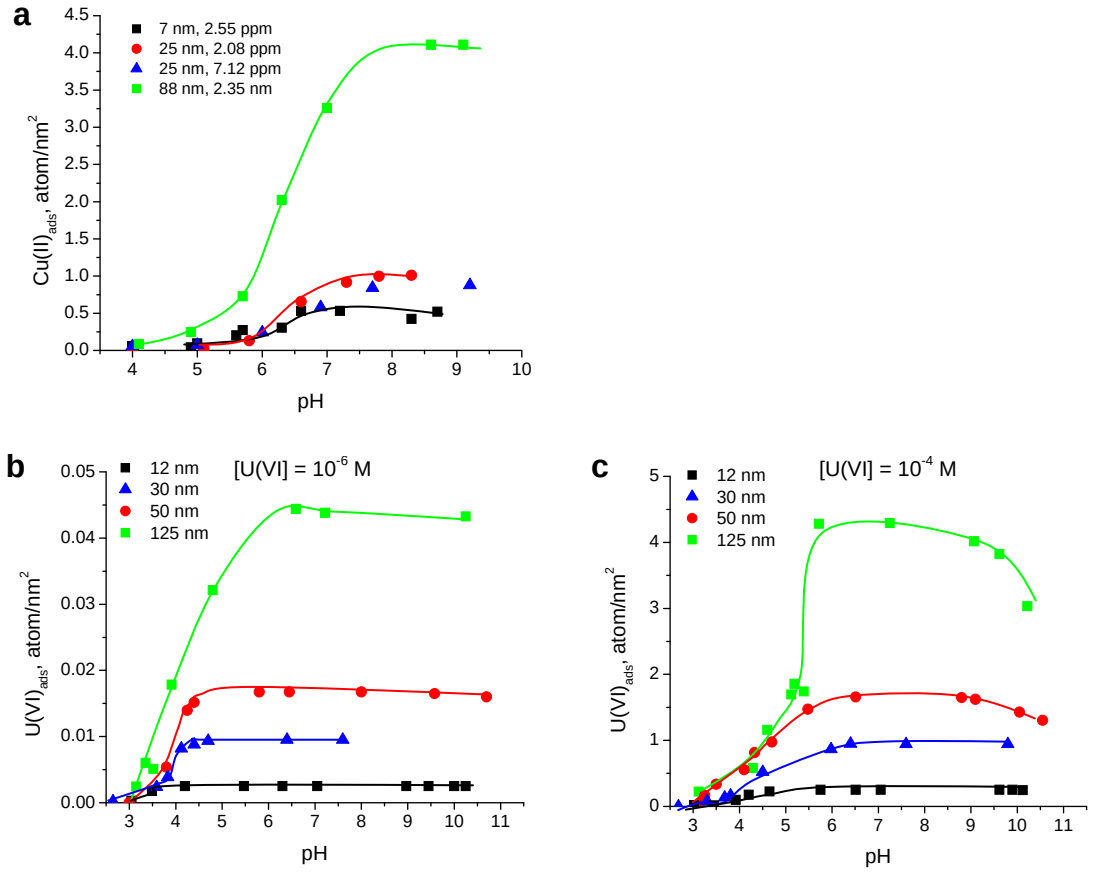

Figure S1. Effect of NP size on surface-area normalized adsorption properties of hematite in the dark: (**a**) Cu(II) sorption density on 7-, 25-, and 88-nm hematite nanoparticles in 0.1 M $NaNO_3$ under N_2-saturated conditions plotted from Table EA1 of Supplementary data of Ref.[1] Total concentration of Cu^{2+} is shown in graph. (**b,c**) U(VI) sorption on 12-, 30-, 50-, 70- and 125-nm hematite nanoparticles synthesized by an aerosol methodin 0.1M $NaNO_3$ replotted on the per surface area basis from Fig. 1b and Fig. 1c of Ref.[2], respectively, at total U(VI) concentration of (**b**) 10^{-6} M and (**c**) 10^{-4} M. Connecting lines are drawn for ease of reading.

Hematite nanoparticles

Two samples of hematite nanoparticles NPs (**H7** and **H9**) were synthesized according to Ref.[3] by slowly dripping 60 mL of 1 M ferric nitrate (Sigma-Aldrich, 99.99% purity) solution into 750 mL of boiling TDW. After the drip solution was consumed, the NP suspension was removed from the heat source. Difference between H7 and H9 was that in the first case heating of the solution was stopped immediately after dripping was started. Third hematite sample **H30** was obtained by the dropwise addition of 40 ml of 0.5 M ferric chloride (Acros, 99+%) into 320 ml of boiling water. **H38** was synthesized according to Ref.[3] by heating 8.08 g of ferric nitrate in 1 L of 0.002 HCl at 98°C. This suspension was aged in the oven at 98°C for 7 d. **H45** was synthesized[4] by adding 25 mL of 0.72M $FeCl_3$ (in 0.001M HCl) to 0.975 L boiling solution of 0.004 M HCl. This suspension at 0.018 M total iron concentration was aged for 24 h at 100° C on a hot plate upon refluxing. **H60** was synthesized by modifying a reported method.[5] A 500 mL solution of 0.2 M ferric nitrate was adjusted to pH 8 with 1 M KOH, and the resulting ferric oxide suspension was heated to 98°C and aged at this temperature for 7 days. After 7 days, the precipitate was dialyzed using singly distilled water and freeze-dried. The XRD of the product revealed hematite with an admixture of goethite. To eliminate goethite this product was dialyzed against water (vide infra), centrifuged, air-dried, and further heated in air for 4h at 500°C. This route gave rhombohedral hematite NPs with mean size of 60 nm as confirmed by TEM and XRD measurements. Sample **H120** was synthesized following a modified procedure described in Ref.[6] A mixture of 0.01M ferric chloride with 0.005M HCl was aged at 98°C for 14 days. In all cases, the precipitation by hydrolysis was followed by cooling the suspensions overnight and dialysis for 2 weeks using singly distilled water until the conductivity of the dialyzed water reached that of the pure water. Sample **H150** synthesized by the annealing of ferric sulfate was purchased from Fisher. 2-line ferrihydrite (**FH**) was purchased from Alfa Aesar as Iron(III) Oxide, 99.95% (metal basis), 3nm APS powder, surface area 250 m^2/g.

Table S1. Morphological characteristics of hematite NPs

Sample	Average Particle Size (TEM), nm	Mean Coherence Length (XRD), nm		Particle Habit (TEM)	BET, m^2/g	GSA, m^2/g	Approximation of shape, height[a] (*h*) in calculating GSA
		(104)	(110)				
FH	2	—	—	[b]	250 [c]	—	—
H7	7	7	[d]	Rounded platelets	154.4	474/214[e]	Hexagonal platelets *h* = 1.5 nm/spheres
H9	9	24/18[f]	25	Rounded platelets	128.3	440/165[e]	Hexagonal platelets *h* = 1.5 nm/spheres
H30	30	26	40	Agglomerates of rounded hexagon-like crystals, porous	56.1	48	Spheres
H38	38	26	45	Hexagons and rhombohedra	37.0	40	Rhombohedra *h* = 26 nm
H45	45	26	36	Rounded rhombohedra, porous	53.8	42/36.3[e]	Rectangular prisms *h* = 26 nm/spheres
H60	60	45	88	Agglomerates of hexagons, porous	65.7	27/23[e]	Rectangular prisms *h* = 45 nm /spheres
H120	120	—	—	Hexagons and rhombohedra	10.0	10.1	Rectangular prisms *h* = 100 nm
H150	150	—	—	Rounded polyhedra	9.5	8.8	Rectangular prisms *h* = 80 nm

[a] Sizes for hexagons, rhombohedra, and rectangles were taken based on the TEM images. Values of *h* for H7 and H9 were approximated by the values provided by AFM for similarly synthesized NPs,[7] for H30–H60 *h* is taken as a mean coherence length in the [104] direction, while for H120 and H150 *h* is taken the average shortest dimension as measured by TEM. Size dependence of the density of hematite NPs was obtained through linear interpolation between values for FH (3.96 g/cm^3) for 2 nm NPs and a bulk value of 5.23 g/cm^3 for 120 nm NPs. [b] Cannot be resolved. [c] Provided by manufacturer. [d] Ratio was not calculated as (110) line is obscured by a 6-line FH peak (Fig. 2); [e] Second value is obtained approximating the NP shape by a sphere with diameter taken as mean coherence length in the [110] direction; [f] Ratio of widths of (024) and (110) lines.

Assignment of ligand field (LF) bands in electronic spectra of hematite NPs

As different from bands *1-7*, band *1'* at ~ 515 nm becomes better resolved with decreasing NP size down from 60 nm and disappear afterwards. This band is attributed to a LF transition in the T_d FeO_4^{5-} groups since LF transitions of T_d Fe^{3+} ions are common in this energy range. [8-11] In particular,

absorption at 510–515 nm is present in spectra of and Fe-doped ZnO (wurtzite) where Fe^{3+} is in tetrahedral co-ordination.[12]

Band *1* at ~ 540 nm (2.3 eV), which is a signature of octahedrally coordinated Fe^{3+} ions in ferrites,[13] was earlier attributed to the $^6A_1 + {}^6A_1 \rightarrow {}^4T_1\,(^4G) + {}^4T_1\,(^4G)$ double exciton process (DEP)[8, 11] and to the $^6A_1 \rightarrow {}^4E$ LF transition in the trigonal LF.[14] We accept the DEP origin of this band because the alternative assignments to single-electron LF transitions, e.g., $^6A_1 \rightarrow {}^4E,{}^6A_1(^4G)$, give essentially larger than 10 nm deviations between the theoretical and experimental positions for other LF bands (*vide infra*).

Band *2* at 486 ± 1 nm was previously observed for polycrystalline hematite films and assigned to the $2t_{2g}\uparrow \rightarrow 2t_{2g}\downarrow$ spin-flip transitions.[14] Alternatively, this band was also hypothesized[15] to be related to 'goethitic' structural components in the Fe-defective hematite NPs. The former assignment is more realistic as no admixture of goethite was detected in the NPs used in the present study both by XRD (*vide supra*) and vibrational spectroscopy.[16] Moreover this band becomes more pronounced with increasing NP size (Fig. 4), i.e., with increasing lattice order. Thus, using the cubic LF notation, band *2* is assigned to the degenerate $^4E,{}^6A_1(^4G)$ spin-flip transition.

Bands *3–7* were further interpreted by fitting their positions into a Tanabe-Sugano (TS) correlation diagram which was constructed for quartet LF states of a ferric ion in the cubic LF[11, 17] at B = 636 cm^{-1} and C/B = 4.48. A good fit obtained between the theoretical and experimental positions (Fig. 4 and Table S1) justified the above interpretation. In fact, bands *3–7* are blue shifted compared to the calculated TS values by not more than ~ 10 nm. The difference can be accounted by the inherent limitations of the TS correlation diagrams.[18]

Table S2. Experimental and theoretical (for H38) positions as well as assignment of components of UV-Vis absorption spectra of aqueous suspensions of hematite NPs. Experimental values were obtained using the 2nd derivatives of the absorption spectra (Fig. 4), theoretical values were obtained using a Tanabe-Sugano (TS) diagram at B = 636 cm^{-1} and C/B = 4.48. Estimated error in band position ±1 nm.

	Band Position, nm										Band Assignment (excited state)	
band	FH	H7	H9	H45	H30	H38		H60	H120	H150	Previous Work	Current Work
						Exptl	Theor					
1	539	537	538	539	541	542	—	541	547	568	DEP[11] ^4E (Ref.[14]) CT,[13, 19] defect states due to O vacancies[20]	DEP
1’	512	516	518	519	518	519	—	519	—	—	—	LF of FeO_4
2	486	485	485	487	486	486	486	486	490	499	spin flip[14], goethite,[15] DEP[9, 21]	spin flip (^4E,$^6A_1$(^4G))
3	425	423	424	425	427	427	436	430	443	449	^4E,$^6A_1$(^4G) (Refs.[11, 8, 22])	CT + $^4T_2$(^4D)
CT2+4	372	365	371	386	386	386	400	390	400	408	CT,[14, 19, 23-27] DEP,[28] $^4T_2$(^4D) + ^4E(^4D) (Ref.[9]) $^4T_2$(^4D) (Ref.[11,8])	CT + ^4E(^4D)
5	323	311	314	318	319	319	329	320	323	327	$^4T_1$(^4P) (Refs.[9, 11]) CT[14, 21]	$^4T_1$(^4P)
6’	—	—	—	—	—	—	295	—	288	290	CT[11, 14]	$^4A_2$(^4F)
CT1+6	270	—	257	260	261	261	270	265	267	270	CT[11, 14]	CT + $^4T_1$(^4F)
7	217	~200	?	217	218	218	230	225	220	227	CT[11, 14]	CT + $^4T_2$(^4F)

XPS analysis

Regional XPS scans within from 10 to 50 eV windows widths were collected at 0.1 eV steps. All samples were prepared by spreading a thin layer of an aqueous suspension of NP on a UHV metallic holder followed by air-drying. XPS spectra for each sample were measured 2–3 times after depositing a fresh layer on the XPS holder. All samples were prepared by spreading a thin layer of an aqueous suspension of NP on a UHV metallic holder followed by air-drying. XPS spectra were measured 2–3 times for each sample freshly deposited on the XPS holder before each measurement. The spectra were reproduced in terms of peak widths and shapes as well surface atomic concentrations, within the experimental error of the method. However, the peak position was reproduced only if binding energies (BE) were corrected for the charging effect by assuming a common BE for the O 1*s* core-level electrons of lattice oxygen, which was taken as 530.1 eV. Such referencing was performed in some of previous XPS studies of ferric oxides.[29, 30] The reason is that common referencing to the C 1*s*

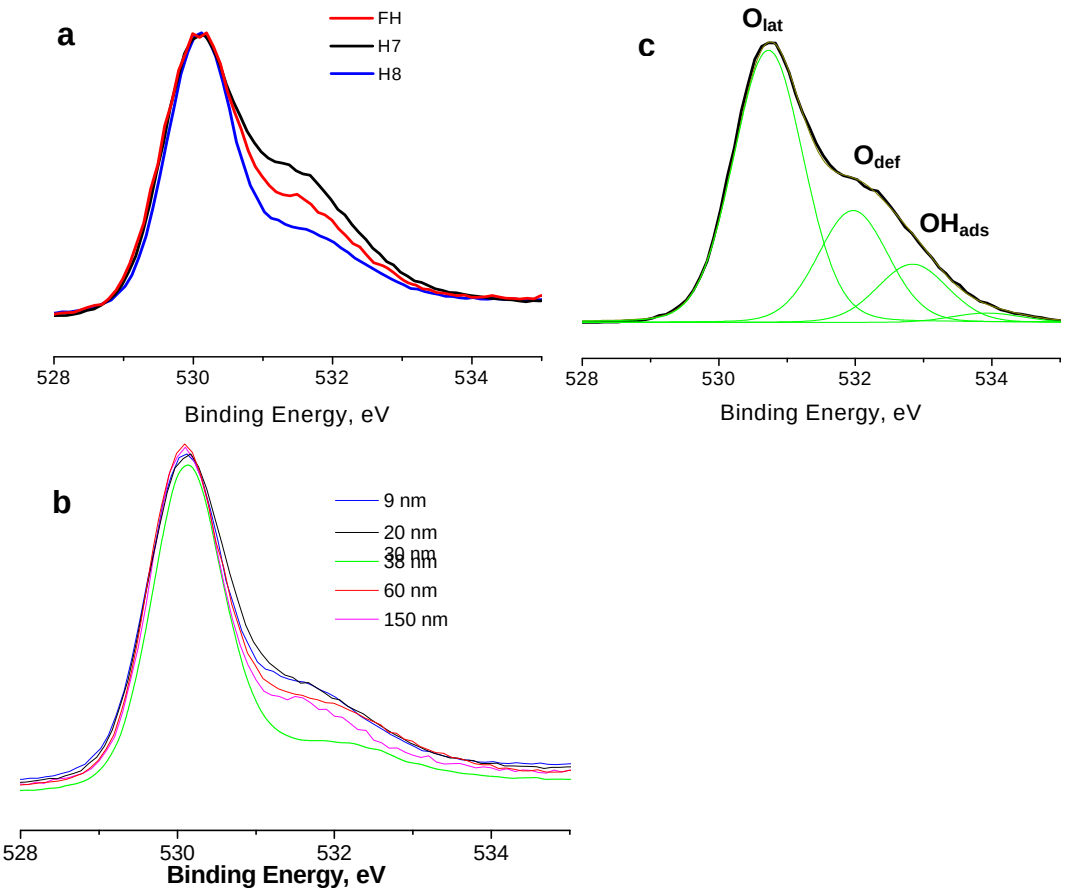

Figure S2. XPS O 1s core level spectra of (*a*) FH (red); H7 (black) and H9 (blue), and (*b*) H9 (blue), H30 (black), H38 (green), H60 (red), H150 (magenta). (*c*) Curve fitting of O 1*s* spectrum of H7.

signal of hydrocarbon contamination can be ambiguous.[31] At the same time, as there is no convincing evidence so far that the O 1*s* peak position of transition metal oxides is significantly affected by cation site occupancy.[32] Shirley function was used to subtract the background. Curve-fitting was performed using a 90% Gaussian-10% Lorentzian function with the full width at half maximum (FWHM) held to be same for all the components of the given peak. O/Fe atomic concentration ratios were evaluated using O 1*s* and Fe $2p_{3/2}$ peaks and PHI atomic sensitivity factors.

The O 1*s* spectra of the ferric oxide NPs (Fig. S2) consist of the principal peak, O_{lat}, at 530.1 eV of oxygen in the hematite lattice and additional components at higher BE. The curve fitting of the O 1*s* spectra can be performed with the minimum number of the additional components of 2 or 3. A component shifted by 1.1–1.4 eV compared to the principal peak is commonly assigned to lattice oxygen in a defective oxide environment[33] and/or lattice hydroxyls (O_{def}).[34] Though adsorbed/incorporated carbonate or carboxylate group of contaminations can also contribute to the O_{def} peak, we neglect this contribution since no correlation was found between intensity of the O_{def} peak with that of the C 1*s* peak at ~289 eV of carbonate. The components shifted by ~2 and ~3 eV can be assigned to surface hydroxyls and physisorbed water, respectively.[33-35] Dependences of the O/Fe atomic ratio for regular lattice O^{2-} and defective lattice O^{2-} are shown in Fig. S3. One can see that the O/Fe ratio for the regular lattice oxygen decreases with decreasing NP size, which may suggest that the surface of larger NPs becomes progressively enriched in iron atoms. At the same time, the relative fraction of oxygen atoms in the lattice defect positions changes non-monotonically, passing through a minimum at ~ 40 nm.

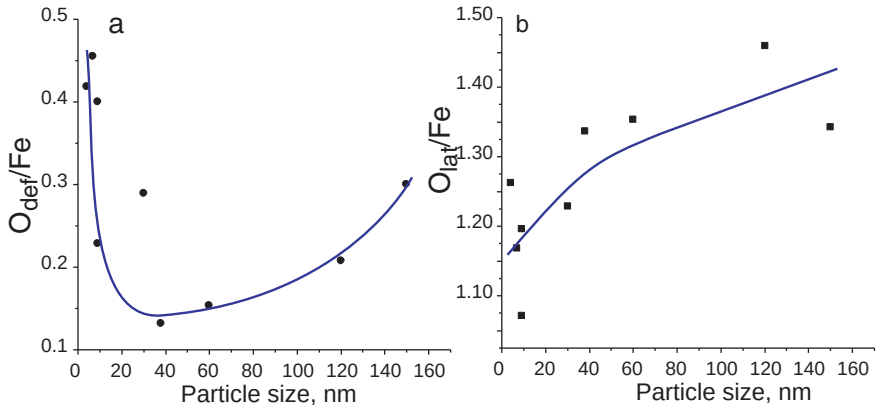

Fig. S3. NP size dependences of the O/Fe atomic ratio for (a) defective lattice O^{2-} and (b) total lattice O^{2-} and in hematite NPs

References

1 A. S. Madden, M. F. Hochella Jr and T. P. Luxton, *Geochim. Cosmochim. Acta*, 2006, **70**, 4095-4104.
2 H. Zeng, A. Singh, S. Basak, K. U. Ulrich, M. Sahu, P. Biswas, J. G. Catalano and D. E. Giammar, *Environ. Sci. Technol.*, 2009, **43**, 1373-1378.
3 U. Schwertmann, Cornell, R.M., *Iron oxides in the laboratory: preparation and characterization*, Wiley-VCH Weinheim, New York, 2000.
4 Y. S. Hwang and J. J. Lenhart, *Journal of Colloid and Interface Science*, 2008, **319**, 206-213.
5 Y. Arai, D. L. Sparks and J. A. Davis, *Environmental Science & Technology*, 2004, **38**, 817-824.
6 S. Music, S. Krehula and S. Popovic, *Materials Letters*, 2004, **58**, 2640-2645.
7 A. S. Madden and M. F. Hochella, *Geochimica Et Cosmochimica Acta*, 2005, **69**, 389-398.
8 M. Lenglet, F. Hochu and Z. Simsa, *Materials Research Bulletin*, 1998, **33**, 1821-1833.
9 T. Y. Chen, C. H. Hsia, H. S. Son and D. H. Son, *Journal of the American Chemical Society*, 2007, **129**, 10829-10836.
10 D. M. Sherman, *Physics and Chemistry of Minerals*, 1985, **12**, 161-175.
11 D. M. Sherman and T. D. Waite, *American Mineralogist*, 1985, **70**, 1262-1269.
12 S. Singh and M. S. R. Rao, *Physical Review B*, 2009, **80**, 10.
13 R. V. Pisarev, A. S. Moskvin, A. M. Kalashnikova and T. Rasing, *Phys. Rev. B*, 2009, **79**, 235128.
14 L. A. Marusak, R. Messier and W. B. White, *Journal of Physics and Chemistry of Solids*, 1980, **41**, 981-984.
15 J. Torrent and V. Barron, *Clays and Clay Minerals*, 2003, **51**, 309-317.
16 I. V. Chernyshova, M. F. Hochella and A. S. Madden, *Physical Chemistry Chemical Physics*, 2007, **9**, 1736-1750.
17 R. V. Morris, H. V. Lauer, C. A. Lawson, E. K. Gibson, G. A. Nace and C. Stewart, *Journal of Geophysical Research-Solid Earth and Planets*, 1985, **90**, 3126-3144.
18 B. Fromme, in *d-d Excitations in Transition-Metal Oxides*, Springer-verlag, Berlin, 2001, vol. 170, pp. 5-26.
19 L. Armelao, M. Bettinelli, M. Casarin, G. Granozzi, E. Tondello and A. Vittadini, *Journal of Physics-Condensed Matter*, 1995, **7**, L299-L305.
20 S. R. Basu, L. W. Martin, Y. H. Chu, M. Gajek, R. Ramesh, R. C. Rai, X. Xu and J. L. Musfeldt, *Appl. Phys. Lett.*, 2008, **92**.
21 S. Music, M. Lenglet, S. Popovic, B. Hannoyer, I. CzakoNagy, M. Ristic, D. Balzar and F. Gashi, *Journal of Materials Science*, 1996, **31**, 4067-4076.
22 Y. P. He, Y. M. Miao, C. R. Li, S. Q. Wang, L. Cao, S. S. Xie, G. Z. Yang, B. S. Zou and C. Burda, *Physical Review B*, 2005, **71**.
23 R. F. G. Gardner, D. W. Tanner and F. Sweett, *Journal of Physics and Chemistry of Solids*, 1963, **24**, 1183-&.
24 T. Hashimoto, T. Yoko and S. Sakka, *Nippon Seramikkusu Kyokai Gakujutsu Ronbunshi-Journal of the Ceramic Society of Japan*, 1993, **101**, 64-68.
25 H. M. Fan, G. J. You, Y. Li, Z. Zheng, H. R. Tan, Z. X. Shen, S. H. Tang and Y. P. Feng, *Journal of Physical Chemistry C*, 2009, **113**, 9928-9935.
26 K. A. Wickersheim and R. A. Lefever, *Journal of Chemical Physics*, 1962, **36**, 844-&.
27 N. C. Debnath and A. B. Anderson, *Journal of the Electrochemical Society*, 1982, **129**, 2169-2174.

28 A. I. Galuza, V. V. Eremenko and A. P. Kirichenko, *Fizika Tverdogo Tela* 1979, **21**, 1125-1129.
29 T. Fujii, F. M. F. de Groot, G. A. Sawatzky, F. C. Voogt, T. Hibma and K. Okada, *Phys. Rev. B*, 1999, **59**, 3195-3202.
30 T. SchedelNiedrig, W. Weiss and R. Schlogl, *Phys. Rev. B*, 1995, **52**, 17449-17460.
31 J. Junta and M. F. Hochella, *Geochim. Cosmochim. Acta*, 1994, **58**, 4985-4999.
32 T. Yamashita and P. Hayes, *J. Electron. Spectrosc. Relat. Phenom.*, 2006, **154**, 41-42.
33 C. Chen, S. J. Splinter, T. Do and N. S. McIntyre, *Surface Science*, 1997, **382**, L652-L657.
34 J. Rakovan, U. Becker and M. F. Hochella, *American Mineralogist*, 1999, **84**, 884-894.
35 A. P. Grosvenor, B. A. Kobe and N. S. McIntyre, *Surface Science*, 2004, **572**, 217-227.